A graphene-based neutral particle detector

J. Warbinek,[1,2] D. Leimbach,[1,2,3] D. Lu,[2] K. Wendt,[1] D.J. Pegg,[4] A. Yurgens,[5] D. Hanstorp,[2] and J. Welander[2]
[1)] *Institute of Physics, Johannes Gutenberg-University, D-55 128 Mainz, Germany*
[2)] *Department of Physics, University of Gothenburg, SE-412 96 Gothenburg, Sweden*
[3)] *CERN, 1211 Geneva, Switzerland*
[4)] *Department of Physics, University of Tennessee, Knoxville TN 37 996, USA*
[5)] *Department of Microtechnology and Nanoscience, Chalmers University of Technology, SE-412 96 Gothenburg, Sweden*

(Dated: 15 October 2020)

A neutral particle detector is presented, in which the traditionally used target material, indium tin oxide (ITO), is replaced by graphene. The graphene-based detector enables collinear photodetachment measurements at a significantly shorter wavelength of light down to 230 nm compared to ITO-based detectors, which are limited at 335 nm. Moreover, the background signal from the photoelectric effect is drastically reduced when using graphene. The graphene-based detector, reaching 1.7 eV further into the UV energy range, allows increased possibilities for photodetachment studies of negatively charged atoms, molecules and clusters.

Detectors for neutral or charged particles are used in a variety of experiments with a broad range of possible projectile energies. In the fields of atomic and molecular physics, particle energies are in the range of a few eV up to a maximum of some tens of keV. Particle energies in the range above some hundred eV can be detected by an electron multiplier device, which is either composed of discrete electrodes denoted as Secondary Electron Multiplier (SEM)[1,2], constructed as continuous-dynode Channel Electron Multiplier (channeltron, CEM)[3] or Micro Channel Plates (MCP)[4]. In all devices, the impact on the first detector surface generates a few secondary electrons by momentum transfer. To prevent pollution or even destruction of the first electrode a self-contained conversion dynode, called the target, is acting as secondary electron emitter for electrons which eventually are detected using the electron multiplying device. In laser particle beam experiments when the cross section of the investigated process is small, a collinear geometry is desirable to increase the interaction volume and hence the signal. Optical transparency of the target electrode is then required if neutral fragments are to be detected[5,6]. The collinear arrangement also significantly reduces the Doppler broadening of any optical excitation process by making use of the velocity bunching phenomenon[7].

One particular type of experiment where merged beams are used is laser photodetachment spectroscopy, in which a negative ion absorbs a photon and breaks up into a neutral particle and a free electron. The rate of neutral particles is then investigated as a function of the laser frequency. Hence, the detector in this experiment has to transmit the laser light without generating the interfering background signal while it must efficiently create secondary electrons by the impinging neutral particles. This is an experimental challenge since a typical laser pulse used in experiments contains 10^{15} photons whereas the typical yield of neutrals could be as low as 0.1 per laser pulse, especially for addressing rare and/or radioactive isotopes[5].

The key component in the design of such a detector is the choice of a suitable target material which must be both transparent over a large wavelength range and electrically conducting to enable electron emission without charging of the surface. However, most materials are either transparent (dielectrics) or conducting (metals). One of the very few materials that possess both characteristics is tin doped indium oxide (ITO or In_2O_3:Sn).

By attaching a thin ITO layer onto a glass plate, a functional detector was designed by Hanstorp[8], which has been used within a variety of experiments[9–11]. The transmission curve for ITO is relatively flat and about 80 % for wavelengths down to 400 nm, after which the transmission drops rapidly[12]. A further complication for experiments with light in the UV range is an intense generation of photoelectrons by the laser pulse passing through the ITO target. Thus, photodetachment studies in collinear geometry with detection of the residual neutral atoms have so far been limited to the visible and infrared spectral regions.

Extending the photon energy range into the UV is of high relevance, for instance in studies of doubly excited states[13,14] or for spectroscopy of molecular negative ions used in accelerator mass spectrometry[15,16]. Hence, alternative target materials have been tested but with limited success. A quartz plate covered with a film of gold has been used[17], but the strong emission of electrons by the laser induced photoelectric effect produced an intensive background that could not be prevented.

An interesting candidate as a target material is graphene. This is a two-dimensional monolayer of sp^2 hybridized carbon atoms with unique mechanical, electronic, and optical properties. It is both electrically conductive and optically transparent with a transmission of 98 % in the visible range and larger than 95 % in the UV region[12]. The high transparency of graphene in the visible range is determined by the fine structure constant and is frequency independent[18]. The slightly smaller transparency in the UV range is due to an excitonic resonance that forms near the van Hove singularity of the band structure of graphene[19].

In this work we present the first investigation when a graphene-coated quartz plate is used as the target in

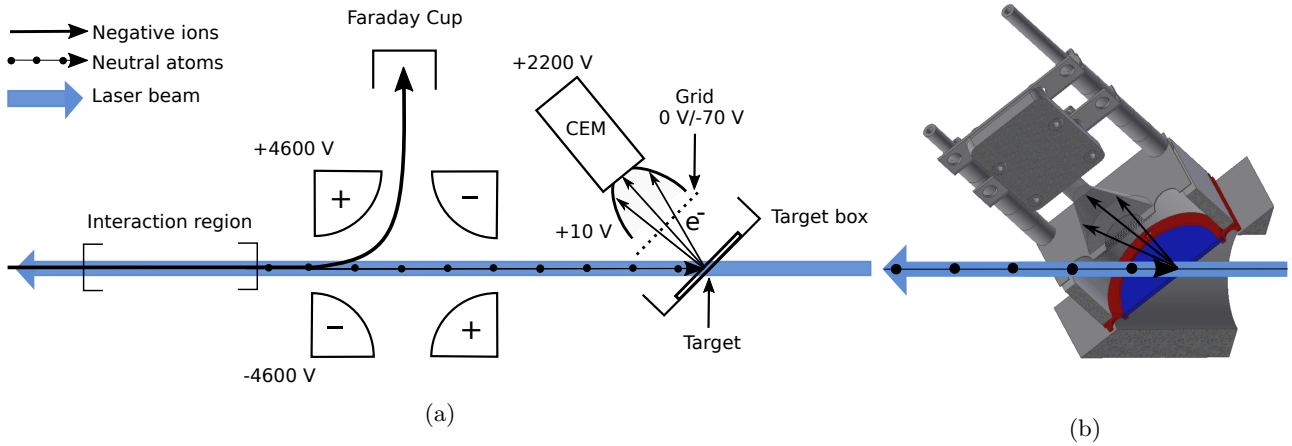

FIG. 1: a) A schematic drawing of the interaction region and the neutral particle detector. A negative ion beam, entering from the left in the figure, is merged with a counterpropagating laser beam in the interaction region. Afterwards, all ions are deflected by a quadrupole deflector into a Faraday cup. Neutralized particles from the photodetachment process impinge on the target where secondary electrons are generated and consequently detected by a CEM. The potential on the metal grid facing the CEM can be switched in order to repel or attract electrons. b) CAD-model of the neutral particle detector with a clear view of the detector box housing the graphene target as well as the CEM entrance cone.

a neutral particle detector, and we demonstrate that it can be used for photodetachment studies covering wavelengths, at least down to 230 nm. The functionality of the detector is demonstrated by successfully detecting the residual atoms produced when photodetaching negative ruthenium ions.

The neutral particle detector is shown schematically in Fig. 1a and the corresponding computer-aided design (CAD) model is shown in Fig. 1b. A negative ion beam is merged with a laser beam in a parallel or anti-parallel geometry within a 0.5 m long interaction region. The vacuum in the experimental chamber is kept at a pressure of 10^{-8} mbar. This ensures that the number of background events created by collisions with residual gas is very small in comparison with the photodetachment signal. The geometry of merged beams provides an extended interaction region and reduces the Doppler broadening due to the velocity compression. The large Doppler shift caused by the high velocity of the ions can easily be compensated by taking the geometric mean of the spectra recorded using parallel and anti-parallel symmetry, respectively[7].

A subsequent quadrupole deflector is used to direct the remaining negative ions into a Faraday cup detector for normalization purposes. However, in the current experiment this normalization was not needed since the acquisition time was sufficiently short to have an essentially stable ion beam current during the entire experiment. The neutral atoms, which are generated in the laser photodetachment process, constitute the signal. They are not affected by the electric fields in the quadrupole deflector. Instead, they enter the detector target box, which is installed downstream, through a 5.0 mm hole and impinge on the target where they generate secondary electrons. These electrons are attracted by a +10 V input potential on the cone of the CEM and subsequently multiplied up to a measurable pulse by the CEM output potential of +2200 V. The CEM is mounted right behind a 10 mm hole facing the target plate. A fast atom impinging on the target will cause a few electrons to be emitted. Each of these electrons can be collected with close to 100 % efficiency by the CEM. The detection efficiency of the CEM is of the order of 80 %. Hence, it is very likely that at least one of the electrons emitted from the surface is detected, resulting in a detector with close to unity detection efficiency[8].

A metal grid is placed between the target plate and the CEM. A potential of 0 V on the grid allows electrons emitted from the target to reach the front of the CEM and hence be detected, whereas a grid potential of -70 V prevents any electrons produced at the target plate to reach the CEM. The potential of the grid is switched from 0 V to -70 V a few nanoseconds before the laser pulse arrives at the target and switched back to 0 V 0.4 µs after the laser pulse. In this way, electrons produced by the direct photoelectric effect on the target are repelled and do not reach the CEM. On the contrary, the neutral particles produced by the photodetachment process in the interaction region arrive at the target a few microseconds after the laser pulse and can hence be detected.

The target is a quartz plate coated with graphene. The CVD-grown monolayer graphene transferred on a $10 \times 10 \times 0.5\,\mathrm{mm}^3$ quartz substrate was purchased from Graphenea (eu.graphenea.com). To ease contacting the graphene, 100/5-nm Au/Cr thin films were deposited at the corners of the substrate by using a shadow mask in an e-beam metal-deposition system.

Experiments to test the performance of the graphene-coated target were performed at the Gothenburg University Negative Ion Laser LAboratory[20] (GUNILLA) using negative ruthenium ions. The ions were photodetached by tunable light from an optical parametric oscillator (OPO) which was pumped by the third harmonic of a Nd:YAG laser, thereby enabling the generation of laser light in a wavelength range of 450 nm-1800 nm. By using frequency doubling the wavelength range was extended down to 230 nm. This laser system has a repetition rate of 10 Hz, a pulse width of 6 ns, a pulse energy of ∼1 mJ and a bandwidth of $0.2\,\mathrm{cm}^{-1}$.

Figure 2 shows the results of the experiment when a beam of negative ruthenium ions was merged with a laser beam at a wavelength of 230 nm. The potential on the grid in front of the CEM is shown in Fig. 2a. As described before, electrons created on the target plate can be detected when the potential on the grid is 0 V but will be suppressed when its potential is at -70 V. In this way the detection of electrons created at the target was blocked for a short time around the arrival of the laser pulse. Figure 2b shows the background due to collisional detachment. This trace was recorded by allowing the continuous ion beam to pass through the interaction region, whereas the laser beam was blocked before entering the vacuum chamber. Pulses with a peak height of more than -15 mV were discriminated for detection. During a period of 12 µs, only a single particle was detected at t = −4 µs.

Figure 2c shows the reversed situation, i.e. when the laser light enters the interaction region, whereas the ion beam is blocked by closing a valve in the beam-line. Even though the CEM is in principle blocked by the repelling potential, the broad peak structure observed around t = 0 µs is caused by the laser light, e.g., by scattering on the grid, where electrons might be produced by the photoelectric effect. These electrons will be attracted by the detector since they are produced at a potential of -70 V, whereas the entrance of the CEM is kept at a potential of +10 V. The signal observed at t = +4 µs is ascribed to background caused e.g., by a dark count in the CEM.

Figure 2d shows the signal when both the ion and laser beams are directed into the vacuum chamber and merged in the interaction region. In this case neutral atoms are created in the interaction region due to the photodetachment process. The arrival time for particles neutralized in the interaction region depends on the acceleration voltage and their mass. In the case of ruthenium ions accelerated to 6 keV, these arrive about 2 µs after the laser pulse. In the data shown in Fig. 2, we observe particles caused by the photodetachment process in the time range of 2 µs-7 µs. In addition, the remaining background signal caused by the laser light at t = 0 µs observed in Fig. 2c and Fig. 2d, can also be seen. The dashed line at t = 1 µs in Fig. 2b-d marks the start of the data taking of the photodetachment signal.

The accumulation of the signal from 200 laserpulses is

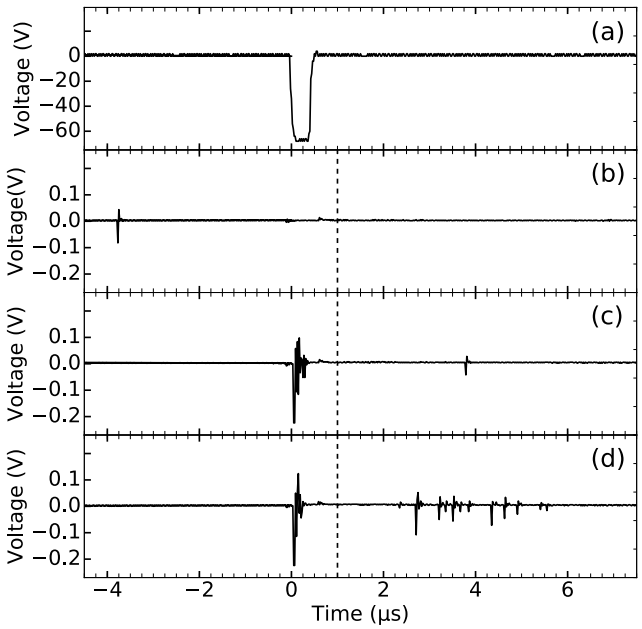

FIG. 2: The time structure of the output from the detector. The laser pulse was triggered at $t = 0$. a) The potential of the metal grid placed in front of the CEM. The output of the CEM when b) the laser beam is blocked but the ion beam is present, c) the ion beam is blocked but the laser beam is directed into the experimental chamber and d) both the ion and laser beams are directed into the vacuum chamber. All traces were recorded with a 250 MHz sampling oscilloscope.

shown in Fig. 3 in form of a histogram in the time range of 1 µs-30 µs with a bin size of 0.5 µs. Figure 3a and Fig. 3b show the signal due to collisional detachment and due to the laser pulse, respectively, while Fig. 3c shows the photodetachment signal. The temporal distribution reflects the spatial overlap of the two beams. The time-of-flight from the interaction region, which is defined by circular apertures, is 2 µs-7 µs. In the case of a perfect collinear overlap of the ion- and laser-beams, one would expect a top-hat distribution in this region. The signal observed at times larger than 7 µs origins from photodetachment in the beam-line where the ions are guided into the interaction region. The signal count rate due to laser induced events is very small in comparison to the photodetachment signals. Note that the scale in Fig. 3a and Fig. 3b is reduced two orders of magnitude in comparison with Fig. 3c. This shows that we can observe the photodetachment process with an almost negligible background from collisional detachment and events caused by the photoelectric effect.

The data shown in Fig. 2 and Fig. 3 were recorded using negative ruthenium ions and a laser wavelength of 230 nm. This wavelength was chosen since this is the shortest wavelength that could be produced in our laboratory and hence also the wavelength where the largest

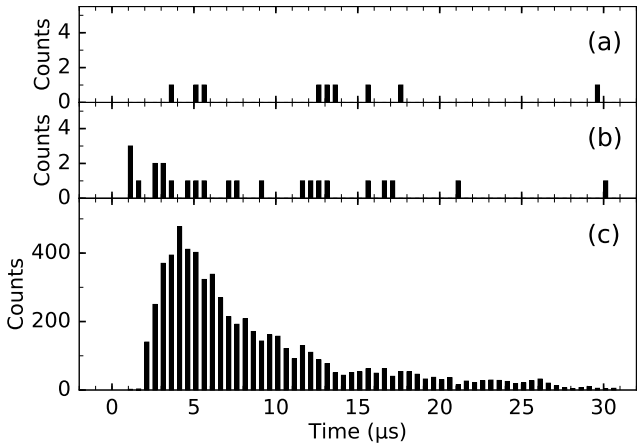

FIG. 3: Histogram of the number of events occurring in the photodetachment experiment. The laser wavelength used was 230 nm. a) Accumulated collisional detachment events recorded with the ion beam present but laser light blocked. b) Accumulated counts with laser light present but ion beam blocked. c) Accumulated photodetachment events recorded with both, ion beam and laser light present.

background would be expected. Furthermore, the detector has been used in other photodetachment experiments using negative ions of iodine, phosphorus and astatine, operating with wavelengths in the ranges 225-350 nm, 404-406 nm, 510-518 nm, and 1100-1400 nm. In no case, any larger background signal than the ones shown in Fig. 3 was observed.

A neutral particle detector based on a graphene-coated quartz plate has been developed for photodetachment studies extending into the UV range. For the lowest accessible wavelength of 230 nm, signals from the photodetachment process were more than two orders of magnitude higher than background from the laser induced photoelectric effect. The recovery time of the CEM after saturation, due to the immediate photoelectric effect, could be reduced to a minimum by rapidly switching the potential on a metal grid placed between the target and the CEM. Due to the high transmission of graphene for UV light, both parallel and anti-parallel alignments of the laser and ion beam are possible.

We have also shown that the graphene-coated target can be used not only using UV laser light, but also in measurements employing visible and infrared laser radiation. It can further be used for detection of any kind of atomic neutral particles with a kinetic energy in the keV range. By replacing the previously used ITO-coated glass target with the graphene-coated quartz, the accessible photon wavelength in the UV range has been extended from 335 nm to 230 nm, which corresponds to an increase of the accessible photon energy of more than 1.7 eV. It should be pointed out that it might be possible to utilize this graphene based detector at even higher photon energies since the upper limit of the photon energy in this work was set by the available OPO laser. Hence, this graphene-based detector design will open up a substantially enlarged energy range for photodetachment studies of negative ions of atoms, molecules and clusters. Based upon the positive characteristics, it was recently installed at the GANDALPH-experiment at CERN-ISOLDE and used to measure the electron affinity of astatine[21].

This work was supported by the Swedish Research Council under Grant No. 2016-03650.

[1] J. S. Allen, "The detection of single positive ions, electrons and photons by a secondary electron multiplier," Phys. Rev. **55**, 966 (1939).
[2] J. S. Allen, "An improved electron multiplier particle counter," Rev. Sci. Instrum. **18**, 739 (1947).
[3] G. W. Goodrich and W. C. Wiley, "Continuous channel electron multiplier," Rev. Sci. Instrum. **33**, 761 (1962).
[4] J. L. Wiza, "Microchannel plate detectors," Nucl. Instrum. Methods **162**, 587 (1979).
[5] S. Rothe, J. Sundberg, J. Welander, K. Chrysalidis, T. Day Goodacre, V. Fedosseev, S. Fiotakis, O. Forstner, R. Heinke, K. Johnston, T. Kron, U. Köster, Y. Liu, B. Marsh, A. Ringvall-Moberg, R. E. Rossel, C. Seiffert, D. Studer, K. Wendt, and D. Hanstorp, "Laser photodetachment of radioactive $^{128}I^-$," J. Phys. G **44**, 104003 (2017).
[6] A. Ellmann, P. Schef, P. Lundin, P. Royen, S. Mannervik, K. Fritioff, P. Andersson, D. Hanstorp, F. C. Fischer, F. Österdahl, D. J. Pegg, N. D. Gibson, H. Danared, and A. Källberg, "Radiative lifetime of a bound excited state of Te^-," Phys. Rev. Lett. **92**, 253002 (2004).
[7] S. L. Kaufman, "High-resolution laser spectroscopy in fast beams," Opt. Commun. **17**, 309 (1976).
[8] D. Hanstorp, "A secondary emission detector capable of preventing detection of the photoelectric effect induced by pulsed lasers," Meas. Sci. Technol. **3**, 523 (1992).
[9] D. Hanstorp and M. Gustafsson, "Determination of the electron affinity of iodine," J. Phys. B: At. Mol. Opt. Phys **25**, 1773 (1992).
[10] K. T. Andersson, J. Sandström, I. Y. Kiyan, D. Hanstorp, and D. J. Pegg, "Measurement of the electron affinity of potassium," Phys. Rev. A **62**, 022503 (2000).
[11] P. Andersson, A. O. Lindahl, D. Hanstorp, and D. J. Pegg, "Observation of the $^2S_{1/2}$ metastable state in Pt^-," Phys. Rev. A **79**, 022502 (2009).
[12] F. Bonaccorso, Z. Sun, T. Hasan, and A. C. Ferrari, "Graphene photonics and optoelectronics," Nat. Photonics. **4**, 611 (2010).
[13] D. J. Pegg, "Structure and dynamics of negative ions," Rep. Prog. Phys. **67**, 857 (2004).
[14] U. Ljungblad, D. Hanstorp, U. Berzinsh, and D. J. Pegg, "Observation of doubly excited states in Li^-," Phys. Rev. Lett. **77**, 3751 (1996).
[15] T. Leopold, J. Rohlén, P. Andersson, C. Diehl, M. Eklund, O. Forstner, D. Hanstorp, H. Hultgren, P. Klason, A. O. Lindahl, and K. Wendt, "Feasibility of photodetachment isobar suppression of WF_5^- with respect to HfF_5^-," Int. J. Mass Spectrom. **359**, 12 (2014).
[16] M. Martschini, J. Pitters, T. Moreau, P. Andersson, O. Forstner, D. Hanstorp, J. Lachner, Y. Liu, A. Priller, P. Steier, and R. Golser, "Selective laser photodetachment of intense atomic and molecular negative ion beams with the ILIAS RFQ ion beam cooler," Int. J. Mass Spectrom. **415**, 9 (2017).
[17] K. C. Chartkunchand, M. Kamińska, E. K. Anderson, M. K. Kristiansson, G. Eklund, O. M. Hole, R. F. Nascimento, M. Blom, M. Björkhage, A. Källberg, P. Löfgren, P. Reinhed, S. Rosén, A. Simonsson, R. D. Thomas, S. Mannervik, V. T. Davis, P. A. Neill, J. S. Thompson, D. Hanstorp, H. Zettergren,

H. Cederquist, and H. T. Schmidt, "Radiative lifetimes of the bound excited states of Pt^-," Phys. Rev. A **94**, 032501 (2016).
[18] R. R. Nair, P. Blake, A. N. Grigorenko, K. S. Novoselov, T. J. Booth, T. Stauber, N. M. R. Peres, and A. K. Geim, "Fine structure constant defines visual transparency of graphene," Science **320**, 1308 (2008).
[19] D.-H. Chae, T. Utikal, S. Weisenburger, H. Giessen, K. v Klitzing, M. Lippitz, and J. Smet, "Excitonic fano resonance in free-standing graphene," Nano Lett. **11**, 1379 (2011).
[20] D. Hanstorp, "An ion beam apparatus for collinear photodetachment experiments," Nucl. Instrum. Methods Phys. Res. Sect. B **100**, 165 (1995).
[21] D. Leimbach, J. Karls, Y. Guo, R. Ahmed, J. Ballof, L. Bengtsson, F. B. Pamies, A. Borschevsky, K. Chrysalidis, E. Eliav, D. Fedorov, V. Fedosseev, O. Forstner, N. Galland, R. F. Garcia Ruiz, C. Granados, R. Heinke, K. Johnston, A. Koszorus, U. Köster, M. K. Kristiansson, Y. Liu, B. Marsh, P. Molkanov, L. F. Pašteka, J. P. Ramos, E. Renault, M. Reponen, A. Ringvall-Moberg, R. E. Rossel, D. Studer, A. Vernon, J. Warbinek, J. Welander, K. Wendt, S. Wilkins, D. Hanstorp, and S. Rothe, Submitted to Nat. Commun.